PCCP

The primary photo-dynamics of lactate in aqueous solution: decarboxylation prevents dehydroxylation

Journal:	*Physical Chemistry Chemical Physics*
Manuscript ID	CP-ART-10-2020-005650.R1
Article Type:	Paper
Date Submitted by the Author:	20-Jan-2021
Complete List of Authors:	ThOgersen, Jan; University of Aarhus, Chemistry Vaida, Veronica; University of Colorado, Department of Chemistry and Biochemistry Bregnhøj, Mikkel; Aarhus University, Chemistry Weidner, Tobias; Max Planck Institute for Polymer Research, Jensen, Frank; Aarhus University, Department of Chemistry

Journal Name

ARTICLE

The primary photo-dissociation dynamics of lactate in aqueous solution: decarboxylation prevents dehydroxylation

Received 00th January 20xx,
Accepted 00th January 20xx

DOI: 10.1039/x0xx00000x

www.rsc.org/

Jan Thøgersen,[a]* Veronica Vaida[b], Mikkel Bregnhøj,[a] Tobias Weidner[a] and Frank Jensen [a]

We study the primary photolysis dynamics of aqueous lactate induced by photo-excitation at λ = 200 nm. Our calculations indicate that both decarboxylation and dehydroxylation are energetically possible, but decarboxylation is favoured dynamically. UV pump - IR probe transient absorption spectroscopy shows that the photolysis is dominated by decarboxylation, whereas dehydroxylation is not observed. Analysis of the transient IR spectrum suggests that photo-dissociation of lactate primarily produces CO_2 and CH_3CHOH^- through the lowest singlet excited state of lactate, which has a lifetime of τ = 11 ps. UV pump – VIS probe transient absorption spectroscopy of electrons from the dissociating lactate anion indicates that the anionic electron from the $CO_2^{\bullet -}$ fragment is transferred to the $CH_3CHOH^{\bullet}$ counter radical during the decarboxylation process, and$CO_2^{\bullet -}$ is consequently only observed as a minor photo-product. The photo-dissociation quantum yield after the full decay of the excited state is Φ(100ps) = 38±5%.

[a] *Dept. of Chemistry, Aarhus University. Langelandsgade 140, DK-8000 Aarhus C, Denmark, E-mail: thogersen@chem.au.dk*
[b] *Department of Chemistry and Biochemistry, CIRES, University of Colorado at*
[c] *Boulder, UCB 215, Boulder, Colorado 80309, USA. E-mail: Vaida@colorado.edu,.*

Introduction

Lactate and lactic acid formed by ultraviolet photolysis of pyruvate are thought to have been among the first organic molecules in the prebiotic waters on Earth and essential to the origin of life. [1-8] In the late Hadean period, the atmosphere mainly consisted of nitrogen and carbon dioxide with smaller quantities of carbon monoxide and hydrogen[9,10] and until the emergence of life, little oxygen and no ozone would have been present. Without the protection of oxygen and ozone, the molecules in the prebiotic waters were exposed to high energy ultraviolet light limited only by water's absorption with an onset around λ = 191 nm. High energy radiation dissociated many prebiotic organic compounds to form reactive radical species, facilitating the formation of complex organics by radical reactions. In the present work, we study the primary photolysis of aqueous lactate when excited at λ = 200 nm with the aim of establishing its photo-stability and primary photo-products.

We have recently reported the primary photolysis of aqueous formate, acetate and propionate as well as alanine, isoleucine and proline when the $n_O \rightarrow \pi_{CO}^*$ transition of these species are excited at λ = 200 nm (E = 6.2 eV).[11,12] All six carboxylates dissociate by decarboxylation via a short-lived lowest singlet excited state as the primary reaction channel. The dissociation dynamics and yields of the six species are nearly identical. Also the calculated excited state surfaces of the six species are quite similar suggesting that $n_O \rightarrow \pi_{CO}^*$ excitation leading to decarboxylation is a general reaction channel for carboxylates. For nearly a century, ultraviolet (λ = 233 – 250 nm) photolysis of lactic acid has been known to produce carbon dioxide and ethanol,[13-18] and drawing on the experience from the other carboxylates, we expect the $n_O \rightarrow \pi_{CO}^*$ excitation of lactate to result in decarboxylation. However, we also present calculations suggesting that in addition to decarboxylation, it is possible that excitation of lactate at λ = 200 nm could also lead to dehydroxylation and we have also considered the possibility of electron detachment. The primary dissociation channels under consideration are shown in Fig. 1.

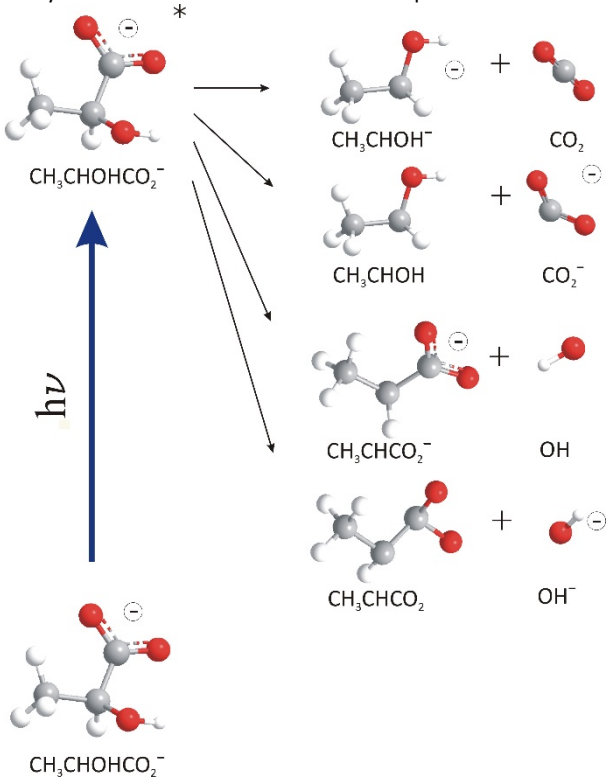

Fig. 1. Potential photo-dissociation channels of aqueous lactate.

Experimental setup

We use sub-picosecond time-resolved absorption spectroscopy to measure the photolysis dynamics of aqueous lactate after femtoseconds of irradiation at λ = 200 nm. The high time resolution enables us to identify the primary reaction products before secondary reactions with other lactate molecules or products from other reaction sites have time to interfere. Two types of transient absorption spectroscopy are utilized in this work.[19] The dynamics of hydrated electrons is studied using UV pump–Vis probe transient absorption spectroscopy, while the dynamics of the molecular products is measured by UV pump–IR probe transient absorption spectroscopy. The λ = 200 nm pump pulses used for exciting the sample are generated in both spectrometers by frequency quadrupling the pulses from a titanium-sapphire laser system running at a pulse repetition rate of f = 1 kHz. A mechanical chopper, phase-locked to the pulse repetition rate, modulates the beam of UV excitation pulses at f = 500 Hz. The excitation pulses are sent via a scanning delay line before a half-wave plate rotates their polarization by θ = 45° and a concave mirror focuses them to a spot size of $2\omega(1/e^2)$ = 160 µm at the sample. Unless other values are noted, the pump pulse duration, spectral width and energy on the sample are τ = 0.2 ps (FWHM), $\Delta\lambda$ = 2 nm and E = 2 µJ, respectively.

The beam of visible probe pulse in the UV-Vis transient absorption spectrometer is generated by frequency doubling the signal beam from an optical parametric oscillator pumped by pulses from the titanium-sapphire laser system. A beam splitter divides the beam of probe pulses into a signal and a reference beam. The signal beam probes the volume excited by the pump pulse while the reference beam passes through the sample outside the excited volume before the two beams are detected by two photodiodes connected to boxcar integrators. A computer normalizes the signal from the signal pulse to that of the reference pulse and calculates the induced transient absorption by subtracting the normalized signal with pump pulse from that without the pump pulse.

The beam of IR probe pulses in the UV pump–IR probe transient absorption spectrometer is generated by difference frequency mixing the signal and idler pulses from an optical parametric amplifier pumped by the titanium-sapphire laser system. A beam-splitter divides the beam of probe pulses into a signal and a reference beam. The signal pulses probe the sample volume excited by the UV pulses, while the reference pulses pass through the sample outside the excited volume. The signal and reference pulses transmitted through the sample are analysed by a polarizer oriented either parallel or perpendicular to the pump beam polarization before they are detected separately by a grating spectrometer equipped with a 2×32-channel HgCdTe dual array detector. A computer normalizes the signal spectrum to the reference spectrum and calculates the

pump-induced transient absorption. The temporal resolution of the spectrometer estimated from the width of the coherence peak recorded in pure water is τ = 0.26ps (FWHM). The data represent the isotropic induced absorption $\Delta A_{iso} = (\Delta A_{\parallel} + 2\Delta A_{\perp})/3$ derived from the absorption transients measured with probe pulse polarizations parallel, $\Delta A_{\parallel}$, and perpendicular, $\Delta A_{\perp}$, to that of the excitation pulse. The uncertainty of the UV-IR transient absorption spectrometer frequency is $\Delta\nu$ ±10 cm^{-1} in the region ν = 1000-2000 cm^{-1} and $\Delta\nu$ = ±5 cm^{-1} in the region ν = 2250-2400 cm^{-1}. The setup is flushed with nitrogen to minimize water vapour and CO_2 in the spectrometer.

The samples consist of a constantly flowing film of aqueous sodium lactate suspended between two parallel, Ø = 50 µm thick tungsten wires separated by d = 4 mm. The flow ensures a fresh sample for every probe pulse. Frequent replacement of the sample reduces the buildup of permanent photoproducts. The lactate samples have concentrations of c = 0.1 M or c = 0.3 M and are dissolved in D_2O or H_2O depending on the spectral region being recorded. The transient data in different spectral regions are recorded using different sample thicknesses and concentrations. The calculated concentration ratio of lactate to lactic acid is ~10^5. The insignificant contribution from lactic acid is supported by the lack of carbonyl transitions in the FTIR and transient absorption spectra of the lactate samples.[20] The aqueous lactate samples are made from sodium lactate with a purity of 99.9 % and with 0.1 % water content. The sodium lactate is purchased from Sigma Aldrich and used as received. The FTIR data of ethoxide is obtained on a sample of ethanol saturated with NaOH.

A Thermo-Fisher 380 ATR-FTIR spectrometer set to a resolution of $\Delta\nu$ = 4 cm^{-1} records the steady state IR spectra of the solutions used for identifying the reaction products. The UV-Vis spectrum of lactate in H_2O is recorded by a Shimadzu UV-3600 double beam spectrometer. The absorbance and wavelength of the Shimadzu spectrometer is calibrated against NaCl(aq) and KCl(aq) certified calibration references (RM-KCSCLCKISI) from Starna.

Theoretical approach

Calculations are done using the ωB97X-D density functional method[21] with the aug-pcseg-1 and aug-pcseg-2 basis sets[22] and the IEFPCM water solvent model, as implemented in the Gaussian16 program package.[23] For some of the calculations, we have additional included explicit water molecules to provide hydrogen bonding to the carbonyl and hydroxyl groups. Excited states are calculated with the time-dependent density functional theory approach and calibration studies suggest a typical accuracy of $\Delta E \sim 0.30$ eV for excitation energies.[24-27] Geometry optimizations and vibrational spectra are done using the aug-pcseg-1 basis set, while the aug-pcseg-2 basis set is used for the excited state results presented in Fig. 2. Excitation energies and electron detachment energies are calculated by the EOM-CCSD and CCSD(T) methods using the aug-cc-pV(D,T,Q)Z basis sets and extrapolated to the basis set limit. The error bars given are estimated from on the basis set convergence. The basis set extrapolated EOM-CCSD excitation energy is 6.23 eV, compared to 5.96 eV calculated at the ωB97X-D/aug-pcseg-2 level. The basis set extrapolated CCSD(T) dissociation energy to CH_3CHOH^- + CO_2 is 3.17 ± 0.01 eV, compared to 3.11 eV calculated at the ωB97X-D/aug-pcseg-2 level (Fig. 2).

Results and discussion

Spectroscopy

The λ = 200 nm excitation wavelength corresponds to a photon energy of 6.2 eV. The lowest calculated vertical excitation energy is 6.0 eV at the ωB97X-D/aug-pcseg-2 level, while the corresponding EOM-CCSD/aug-cc-pV(T,Q)Z extrapolated value is 6.2 eV. Fig. 2a shows the ground and five lowest singlet excited states as a function of the C-CO_2 distance with all other geometry parameters optimized on the ground state energy surface. Fig. 2b shows the corresponding energy curves as a function of the C-OH distance with all other geometry parameters optimized on the ground state energy surface. These figures show that 200 nm excitation can populate a number of closely lying excited states, all of which can be classified as $n_O \rightarrow \pi_{CO}^*$. We assume that population of any of these states rapidly decays to the lowest excited state, where the subsequent nuclear motion takes place. Fig. 2c shows the calculated adiabatic (geometry-relaxed) energy profile for the ground and lowest singlet excited states as a function of both the C-CO_2 and C-OH distance, corresponding to dissociation of either CO_2 or OH. Fig. 2a,b,c in combination show that vertical excitation of lactate occurs at a geometry where dissociation of CO_2 can take place on the excited state surface essentially without a barrier by simply elongating the C-CO_2 bond. The adiabatic energy curve along the C-OH bond in Fig. 2c shows that dissociation of OH can also occur with a very small energy barrier, but Fig. 2b shows that this requires changes in coordinates other than the C-OH bond, as simple C-OH bond elongation leads to a substantial energy barrier. In combination, these figures show that both CO_2 and OH dissociation are possible by energetic criteria, but CO_2 dissociation is expected to be favored by dynamical factors. We note that the geometry relaxed excited state is 4.9 eV above the ground state, and the excitation energy of 6.2 eV thus leaves sufficient kinetic energy in the system to overcome the ~ 0.3 eV energy barrier for CO_2 dissociation.

Electron detachment is a possible competing process, but CCSD(T)/aug-cc-pV(T,Q)Z calculations suggest that this requires 6.6 ± 0.1 eV, and the value is increased to 7.2 eV if three explicit water molecules are included in the calculations. Although these are vertical values, and thus do not include thermal energies, they suggest that electron detachment is unlikely on an energetic criterion. The calculations thus imply that both decarboxylation and dehydroxylation are energetically feasible, whereas electron detachment is not, and that decarboxylation is expected to dominate for dynamical reasons.

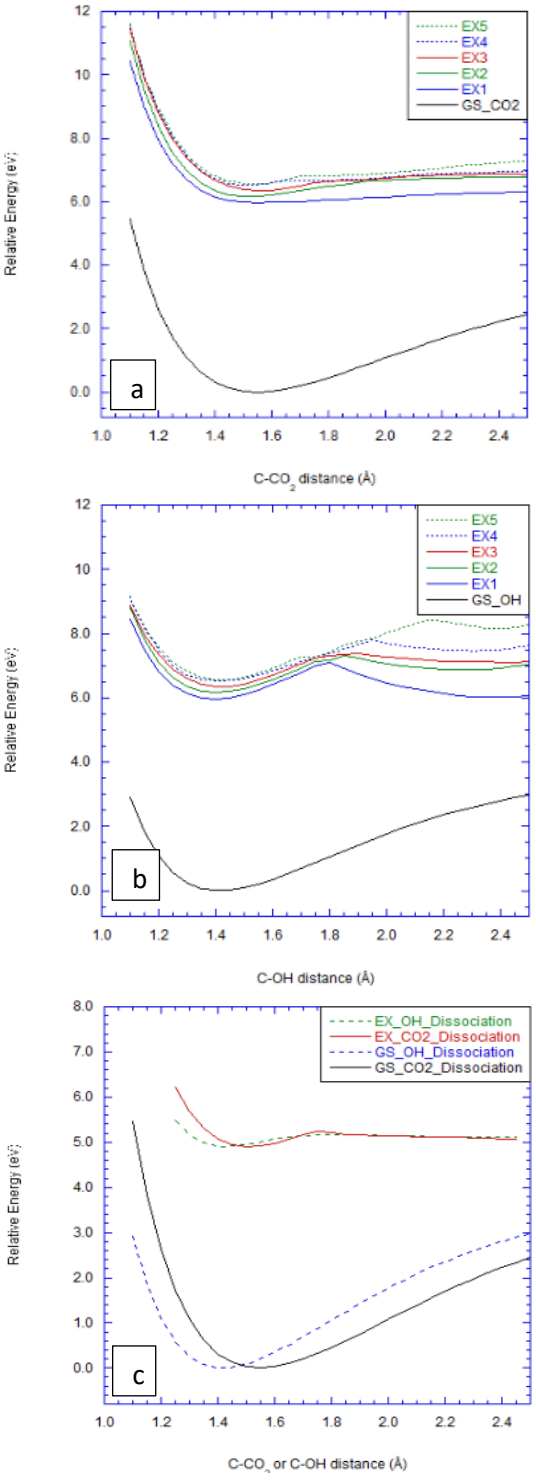

Fig. 2. a: Ground and five lowest excited states along the ground state relaxed geometry corresponding to CO_2 dissociation. b: Ground and five lowest excited states along the ground state relaxed geometry corresponding to OH dissociation. c: Calculated adiabatic (geometry-relaxed) energy profiles for the ground and lowest excited states corresponding to dissociation of either CO_2 or OH.

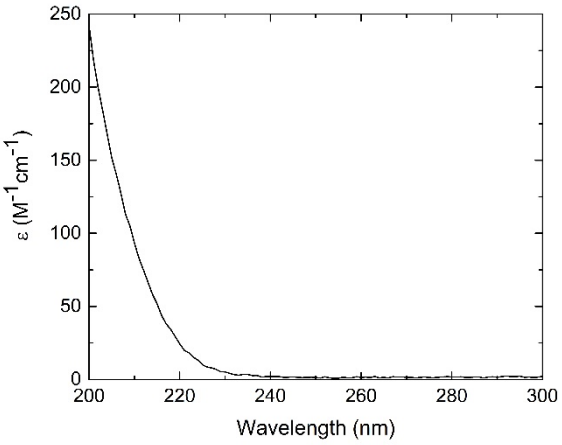

Fig. 3. Absorption spectrum of lactate in H_2O.

Fig. 3 shows the ultraviolet absorption of lactate dissolved in H_2O. Lactate has only one absorption band within water's transmission window. The extinction coefficient is $\varepsilon = 240 \pm 20\ M^{-1}\ cm^{-1}$ at $\lambda = 200$ nm and drops off to less than $\varepsilon = 5\ M^{-1}\ cm^{-1}$ at wavelengths longer than $\lambda = 235$ nm. The $\lambda = 200$ nm pump pulse excites the lactate anions close to the highest absorption within the water transmission window.

UV pump–IR probe transient absorption spectroscopy measures the vibrational transition frequencies and intensities of the products induced by the UV pump pulse as a function of time between pump and probe pulses. This enables the observation of short-lived transient species, but identifying the actual chemical species responsible for the observed vibrational transitions requires an external calibration. This can be either experimental observations of relevant stable species or calculated spectra of transient intermediates. Calculated spectra rarely provide the same accuracy as experimental results, but the expected accuracy can be established by calibration of the employed method against experimental data.

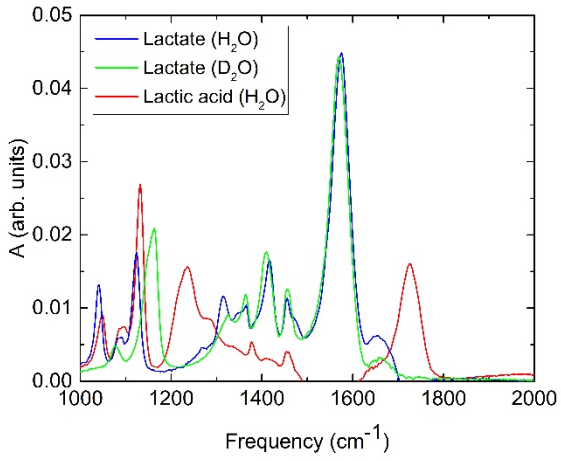

Fig. 4. ATR-FTR spectra of lactate and lactic acid.

Fig. 4 shows the infrared absorption spectra of lactate dissolved in H_2O and D_2O. Table 1 lists selected experimental and calculated transition frequencies for aqueous lactate in the electronic ground state and lowest singlet excited state. The transition associated with the asymmetric CO_2^- stretch is at ν = 1575 cm^{-1} in H_2O and ν = 1570 cm^{-1} in D_2O. The transitions at ν = 1460 cm^{-1} and ν = 1415 cm^{-1} in H_2O are assigned to vibrations of the CH_3 group. The hydrogen atoms of CH_3 are not exchanged in D_2O and the frequencies of the CH_3 transitions are therefore basically the same in both solvents. The transitions at ν = 1390 cm^{-1} in both H_2O and D_2O pertain to the symmetric CO_2^- stretch vibration, while the transition at ν = 1365 cm^{-1} is associated with the bending vibration of the CH group. The transition at ν = 1315 cm^{-1} and ν = 1285 cm^{-1} in H_2O and 1320 cm^{-1} in D_2O are assigned to a mix of CH_3 and OH bending and the transition at ν = 1270 cm^{-1} is due to bending of the CH group. The transition at ν = 1125 cm^{-1} in H_2O and ν = 1163 cm^{-1} in D_2O are assigned to CO stretching transitions, while the transitions at ν = 1090 cm^{-1} and ν = 1045 cm^{-1} are associated with stretching of the CC bond. In acidic solution, the carboxylate CO_2^- group becomes protonated and the CO_2^- related transitions at ν = 1575 cm^{-1} (H_2O) and ν = 1570 cm^{-1} (D_2O) together with ν = 1390 cm^{-1} (H_2O, D_2O) therefore disappear. Instead, carboxyl acid COOH/COOD transitions appear at ν = 1720 cm^{-1} and ν = 1230 cm^{-1}. The calculated anharmonic frequencies with three explicit water molecules listed in Table 1 overestimate the measured CO_2^- asymmetric stretch and CH bend transition frequencies by 2 %, while the average accuracy is 1%.

If photo-excitation of lactate at λ = 200 nm results in decarboxylation, the primary products are the CO_2 molecule and the CH_3CHOH^- anion. Alternatively, the electron may stay on CO_2 during the dissociation in which case $CO_2^{\bullet -}$ and the $CH_3CHOH^\bullet$ radical are formed. CO_2(aq) is identified by its strong transition at ν = 2343 cm^{-1} with a calculated intensity of 826 km/mol associated with its asymmetric stretch,[28] while $CO_2^{\bullet -}$(aq) radical anion is identified by its asymmetric stretch transition around ν = 1650 cm^{-1} known from matrix studies[29-31], aqueous solution[32] and the photolysis of aqueous formate.[33] This transition has a calculated intensity of 528 km/mol. Electron detachment will lead to formation of the lactate radical. Our calculations show that this in a barrier-less reaction dissociate into CO_2 and the $CH_3CHOH^\bullet$ radical. Table 2 lists the calculated transition frequencies of CH_3CHOH^- and $CH_3CHOH^\bullet$ in the ν = 1000 - 2000 cm^{-1} region. The vibrational transition frequencies of the electronically excited state of aqueous lactate have not been determined experimentally, and the identification of the lowest excited state therefore has to rely on the calculated frequencies listed in Table 1.

Table 1. Calculated transition frequencies, ν (cm^{-1}), and intensities, I (km/mol), at the ωB97X-D/aug-pcseg-1 level using the IEFPCM continuum water solvent model in the ν = 1000-2000 cm^{-1} region. Calculated frequencies are harmonic with anharmonic values in parenthesis, with three explicit water molecules for the ground and excited state of $CH_3CHOHCO_2^-$, and with two explicit water molecules for $CH_3CHCO_2^{\bullet -}$ and CH_3CHCO_2. The experimental transition frequencies are determined by ATR-FTIR spectroscopy. The assignment of the measured transitions to vibrational normal modes is based on our calculations, and they largely agree with the assignments of ref. 34

	$CH_3CHOHCO_2^-$ ground state				$CH_3CHOHCO_2^-$ exc. state		$CH_3CHCO_2^{\bullet -}$		CH_3CHCO_2	
	Measured		Calculated		Calculated		Calculated		Calculated	
	H_2O	D_2O	H_2O		H_2O		H_2O		H_2O	
Vib. mode	ν		ν	I	ν	I	ν	I	ν	I
νCO									1986 (1927)	813 (429)
$\nu_{as}CO_2^-$	1575	1570	1634 (1613)	759 (200)	1135	47	1582 (1550)	957 (468)		
$\delta_{as}CH_3$	1460	1456	1498 (1461)	185 (67)	1490	20	1477 (1242)	199 (38)	1479 (1397)	10 (7)
δCH_3	1415	1411	1379 (1425)	26 (11)	1482	14	1453 (1493)	12 (24)	1462 (1436)	6 (5)
$\nu_sCO_2^-$	1390	1390	1458 (1423)	116 (4)	1409	92	1434 (1557)	162 (213)	1409 (1348)	25 (13)
δCH	1365	1365	1437 (1397)	158 (94)	1340	11			1374 (1282)	35 (29)
δCH_3+δOH	1315	1320	1391 (1354)	16 (7)	1382	33				
δCH_3+δOH	1285		1334 (1284)	3 (3)	1447	61				
δCH	1270		1309 (1275)	24 (4)	1325	8	1313 (1307)	248 (134)	1252 (1182)	131 (98)
νCO	1125	1163	1155 (1123)	190 (86)	1114	186	1385 (1482)	78 (28)	1172 (1106)	123 (25)
νCC	1090	1080	1107 (1098)	7 (3)	1082	21	1149 (1139)	5 (1)	1123 (1031)	22 (10)
νCC	1045		1059 (1041)	89 (43)	1016	70	1053 (1050)	16 (7)	1048 (991)	56 (31)

Table 2. Calculated transition frequencies, ν (cm^{-1}), and intensities, I (km/mol), at the ωB97X-D/aug-pcseg-1 level using the IEFPCM continuum water solvent model in the ν = 1000-2000 cm^{-1} region. Calculated frequencies are harmonic with anharmonic values in parenthesis, with one explicit water molecule for $CH_3CHOH^{\bullet}$ and $CH_3CH_2O^-$. CH_3CHOH^- is a sufficiently strong base that it abstracts a proton to form ethanol if an explicit water molecule is included. The calculated energy difference between anti and syn CH_3CHOH^- is insignificant compared to kT, and the listed transition frequencies are therefore the average of the calculated frequencies for the two configurations. Likewise, the calculated energy difference between anti and gauche ethanol is insignificant compared to kT, and the calculated transition frequencies are therefore the average of the calculated frequencies for the two configurations. The experimental transition frequencies are determined by ATR-FTIR spectroscopy. The assignment of the measured transitions to vibrational normal modes for ethanol is based on our calculations, and they largely agree with the assignments of ref. 35.

	CH_3CHOH^-		$CH_3CHOH^{\bullet}$		$CH_3CH_2O^-$			CH_3CH_2OH		
	Calculated		Calculated		Calculated		Measured	Calculated		Measured
Vib.	ν	I	ν	I	ν	I	ν	ν	I	ν
δCH_2					1495 (1454)	27 (2)	1483	1504 (1473)	3 (3)	1482
$\delta_a CH_3$	1480 (1417)	17 (14)	1474	21	1470 (1412)	5 (4)	1441	1476 (1455)	4 (9)	1454
$\delta_a CH_3$	1441 (1385)	4 (4)	1452	15	1458 (1412)	6 (4)	1425	1470 (1439)	10 (5)	-
Mix			1464	152				1440 (1407)	40 (19)	1417
δCH_2					1396 (1352)	159 (36)	1375			
$umCH_3$	1371 (1317)	13 (8)	1398	1	1366 (1324)	14 (15)	1354	1391 (1387)	5 (5)	1386
δCH_2					1294 (1260)	14 (6)	1277	1337 (1313)	2 (3)	1324
δCH	1351 (1292)	5 (3)								
δOH	1225 (1147)	46 (24)	1351	11				1277 (1278)	57 (42)	1276
δCH_2								1155 (1140)	9 (11)	1160
Mix	1124 (1062)	17 (3)	1031	82	1169 (1121)	14 (32)	1160			
νC-O			1233	169	1145 (1094)	332 (182)	1093	1105 (1077)	107 (93)	1090
νC-C			1097	33	1079 (1045)	122 (124)	1049	1062 (1063)	59 (35)	1045

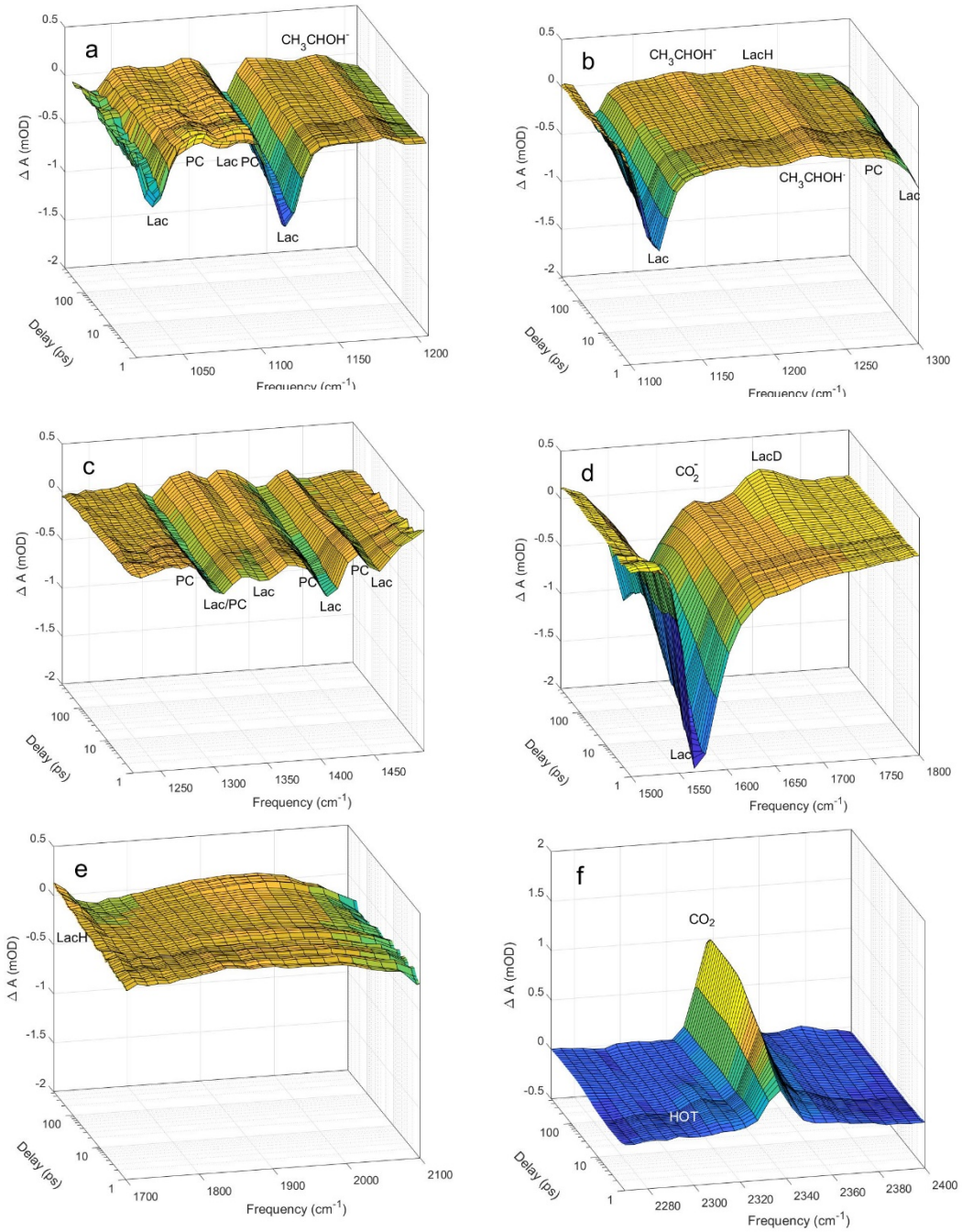

Fig. 5 Transient absorption spectra of aqueous lactate as a function of time after the λ = 200 nm excitation pulse. Notation: PC: precursor, Lac: lactate, LacH: Lactic acid, LacD: Lactic acid (D), HOT: CO_2 hot bands. a) The negative absorption associated with the νCC transition of lactate at ν = 1034 cm^{-1}, the νCC transition of lactate at ν = 1082 cm^{-1} and the νCO transition of lactate at ν = 1117 cm^{-1}. The precursor gives rise to a positive, short-lived absorption at ν = 1060 cm^{-1} and ν = 1094 cm^{-1}. The positive absorption at ν = 1180 cm^{-1} is assigned to the δOH of CH_3CHOH^-. b) The positive absorption at ν = 1230 cm^{-1} is assigned to the νCO transition of $CH_3CHOH^•$ and the C-OH stretch transition of lactic acid, while the precursor induces a short-lived positive absorption at ν = 1270 cm^{-1}. c) The negative absorptions at ν = 1309 cm^{-1}, ν = 1351 cm^{-1}, ν = 1397 cm^{-1}, ν = 1415 cm^{-1} and ν = 1455 cm^{-1} are due to the δOH+δCH_3, δCH, $\nu_s CO_2^-$, δCH_3, and $\delta_{as} CH_3$ transitions of lactate, respectively. The precursor is seen as the short-lived positive absorption at ν = 1301 cm^{-1}, ν = 1387 cm^{-1} and ν = 1435 cm^{-1}, while the positive absorption peaks at long delays at ν = 1333 cm^{-1} and ν = 1435 cm^{-1} are assigned to the $um CH_3$ and $\delta_a CH_3$ transitions of CH_3CHOH^-, respectively. d) The negative induced absorption at ν = 1570 cm^{-1} is associated with the $\nu_{as} CO_2^-$ transition of deuterated lactate and the increasing positive absorption at ν = 1650 cm^{-1} is assigned to $\nu_{as} CO_2^-$ transition of $CO_2^{•-}$, while the slowly increasing, positive absorption at ν = 1720 cm^{-1} pertains to the carbonyl stretch transition of deuterated lactic acid. e) No transitions are observed in the region ν = 1750-2100 cm^{-1}. f) The CO_2 asymmetric stretch transition in H_2O at ν = 2343 cm^{-1} with a hot band at ν = 2315 cm^{-1}. The spectra a-c) and e-f) are recorded in H_2O, while d) is recorded in D_2O. The first t = 30 ps of the data are shown on a linear time axis in ESI.

Fig. 5 shows the complete set of transient infrared absorption spectra while Fig. 6 presents selected close-ups of the transients from Fig. 5. The solvent background has been subtracted from the data. Positive ΔA values indicate the formation of new species, while negative ΔA values imply the excitation of ground state lactate. The data measured for -1 < t < 1 ps are obscured by the t = 0 coherence signal and Fig. 5 and Fig. 6 therefore only show data after 1 ps. Separate measurements of the pump pulse energy dependence of the transient absorption of ground state lactate (see ESI) demonstrate that the excitation of lactate increases linearly with pump pulse energy and that the absorption dynamics during the first t ~50 ps is independent of the pump pulse energy. Accordingly, the induced transient absorption is primarily due to one-photon excitation.

Excitation of ground state lactate

All the major transitions of ground state lactate appear in Fig. 5 as negative induced absorption peaks. The negative absorption associated with the νCC transition of lactate is at ν = 1034 cm^{-1}, the νCC transition of lactate at ν = 1082 cm^{-1} and the νCO transition of lactate is observed at ν = 1117 cm^{-1}. The negative absorption observed at ν = 1309 cm^{-1}, 1351 cm^{-1}, 1397 cm^{-1}, 1415 cm^{-1} and 1455 cm^{-1} are due to the δCH_3+δOH, δCH, $\nu_s CO_2^-$, δCH_3 and $\delta_{as} CH_3$ transitions of lactate, respectively. The weak transitions at ν = 1270 cm^{-1} and 1285 cm^{-1} from the δCH and δCH_3+δOH transitions recorded by ATR-FTIR are below the detection limit of the transient absorption spectrometer, and therefore not observed. The negative induced absorption at ν = 1570 cm^{-1} in D_2O is associated with the $\nu_{as} CO_2^-$ transition of deuterated lactate. The negative absorption transients drop to a minimum immediately after the excitation pulse and then partially recover on a τ = 10 ps timescale reflecting the excitation from, and subsequent partial return to, the electronic ground state of lactate.

Photoproducts

Positive absorptions indicate formation of new species and Fig. 5 shows seven positive absorption peaks after t = 500 ps, where the peaks at ν = 1230 cm^{-1} and 1720 cm^{-1} appearing at long delays are associated with the C-OH stretch and the carbonyl stretch transitions of lactic acid (D), respectively. The absorption at ν = 1230 cm^{-1} has an early component, which we assign to the νC-O stretch transition of $CH_3CHOH^{\bullet}$. The absorption at ν = 1650 cm^{-1} and 2343 cm^{-1} are due to the asymmetric stretch transitions of $CO_2^{\bullet-}$ and CO_2, respectively, while the absorptions at ν = 1180 cm^{-1}, 1333 cm^{-1} and 1435 cm^{-1} are assigned to the δOH, umCH_3 and $\delta_a CH_3$ transitions of CH_3CHOH^-, respectively. The absorption peaks pertaining to CO_2, $CO_2^{\bullet-}$, $CH_3CHOH^{\bullet}$ and CH_3CHOH^- are present after τ = 1 ps. The CO_2 peak increases to a constant level on a 11 ps timescale, while the statistics of the $CO_2^{\bullet-}$, $CH_3CHOH^{\bullet}$ and CH_3CHOH^- peaks are insufficient for a proper determination of the time constants for their increase.

Fig. 5 in addition reveals six short-lived positive absorption transients at ν = 1060 cm^{-1}, 1094 cm^{-1}, 1270 cm^{-1}, 1301 cm^{-1}, 1387 cm^{-1} and 1435 cm^{-1}. They appear immediately after the excitation pulse, grow to a maximum in t = 1-5 ps and then disappear on a 11 ps timescale. The species responsible for these short-lived transients will be referred to as a precursor (PC). In the following sections, we justify the assignment of the photoproducts and identify the precursor.

Protonation by secondary reactions

The absorption peak associated with the vibrational transitions at ν = 1720 cm^{-1} is undetectable during the first 50 ps after the excitation pulse, but then increase with a time constant of ~100 ps for the subsequent 400 ps. The delayed appearance of the absorption peak suggests it is associated with species produced in secondary reactions. We have previously studied the delayed appearance of similar absorption peaks following the photolysis of aqueous alanine at λ = 266 nm and aqueous amino acids and carboxylates at λ = 200 nm.[11, 12, 36] The absorption peaks in those studies originated from protonated amino acids and protonated carboxylates, respectively, and were formed when hydronium ions generated by two-photon ionization of water reacted with the carboxylate group. The ν = 1230 cm^{-1} and 1720 cm^{-1} absorption peaks observed in the present study are in perfect agreement with those of the C-OH stretch transition and the carbonyl stretch transition of lactic acid shown in Fig. 5. Based on the strong similarity with the absorption dynamics pertaining to the protonation of amino acids and carboxylates, we assign the peaks to lactic acid formed when hydronium cations generated by two-photon ionization of water react with lactate. The protonation results in a relatively slow decrease in the concentration of ground state lactate anions, and this causes a second drop in the negative induced absorption of ground state lactate, as observed at the symmetric and asymmetric CO_2^- stretch transitions of lactate at ν = 1397 cm^{-1} and 1570 cm^{-1}, respectively. In agreement with this assignment, the induced absorption decreases on the same timescale as the induced absorption of lactic acid at ν = 1720 cm^{-1} increases. The lactate transition dynamics at ν = 1034 cm^{-1}, 1082 cm^{-1} and 1117 cm^{-1} do not display the same second drop because the absorption associated with lactate and lactic acid are comparable at these frequencies. The late transitions at ν = 1230 cm^{-1} and 1720 cm^{-1} are therefore not caused by photo-excitation of lactate anions, but are due to competing secondary reactions between photo-ionized water molecules and ground state lactate anions. The onset of one-photon absorption of water coincides with its ionization threshold of 6.5 eV (λ = 191 nm). One-photon ionization of water at λ = 200 nm is thus insignificant, whereas the two-photon ionization is not.[37] Accordingly a substantial fraction of the water molecules are two-photon ionized. In contrast, one-photon absorption by lactate completely dominates over a two-photon excitation, and the non-linear contribution to the transient absorption of lactate is therefore insignificant. The reader is referred to the *Electron detachment* section below, to the ESI and to reference 37 for a more thorough discussion.

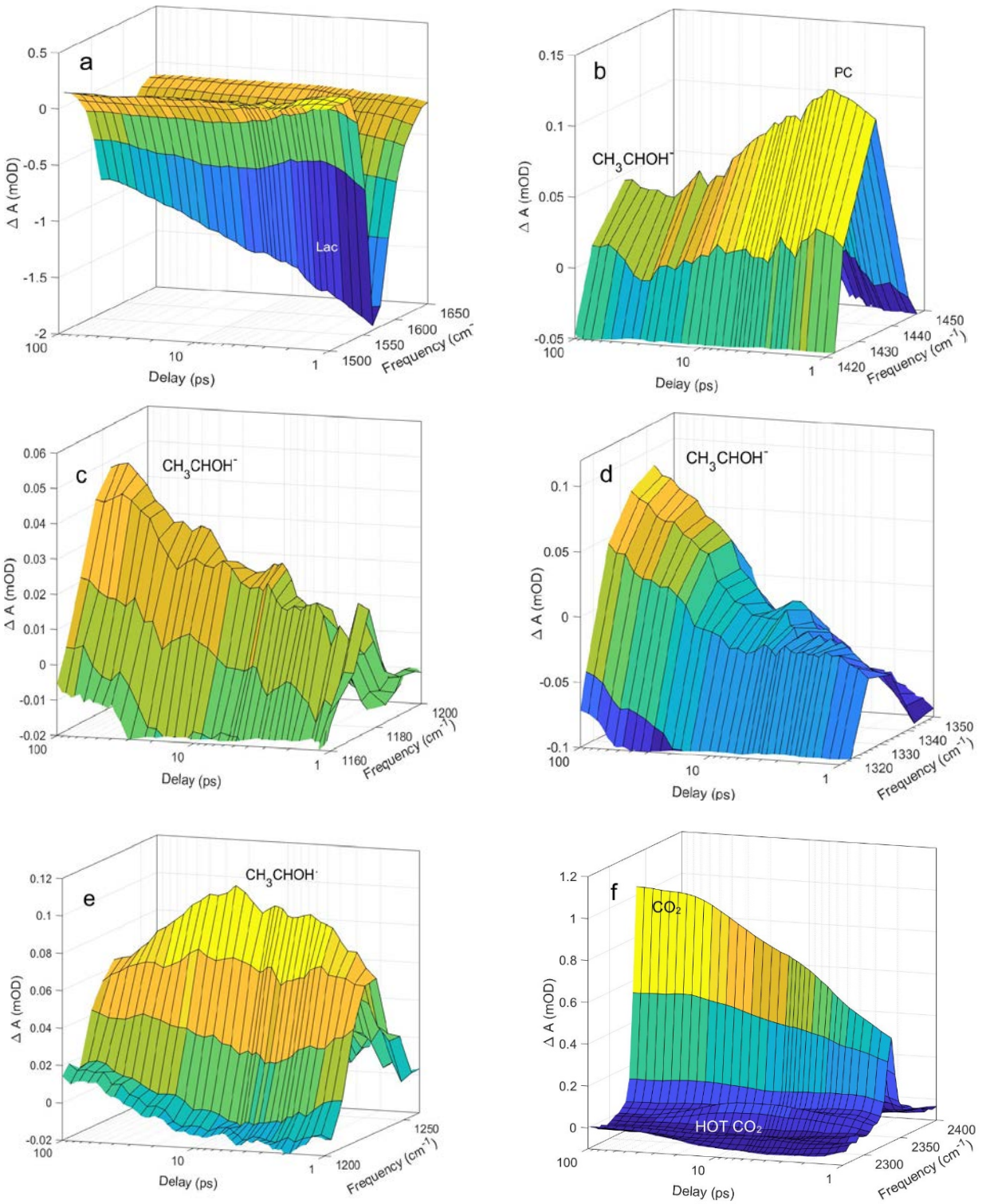

Fig. 6. The first t = 100 ps of the absorption dynamics of a) Ground state lactate represented by the asymmetric stretch transition at ν = 1570 cm^{-1} . b) The lowest singlet excited electronic state of lactate (PC) exemplified by the transition at ν = 1435 cm^{-1} and the absorption of the emerging CH_3CHOH^- anion at the same frequency. c) The CH_3CHOH^- anion represented by its δOH transition at ν = 1180 cm^{-1}. d) The CH_3CHOH^- anion represented by the umCH_3 transition at ν = 1333 cm^{-1}. e) The $CH_3CHOH^•$ radical represented by absorption associated with νCO stretch at ν = 1230 cm^{-1}. f) CO_2 represented by its absorption pertaining to the asymmetric stretch at ν = 2343 cm^{-1}. More figures in ESI.

Decarboxylation

Fig. 5f and Fig. 6f show a strong induced absorption at ν = 2343 cm^{-1}. This frequency is identical to the fundamental transition frequency of the asymmetric stretch vibration of $CO_2(aq)$[28] and the dynamics of the absorption is similar to that of $CO_2(aq)$ resulting from photo-decarboxylation of carboxylates and amino acids reported

earlier,[11,12] and we therefore assign the ν = 2343 cm^{-1} absorption to aqueous CO_2. The absorption reaches 1/3 of its final value within 1 ps after the excitation pulse and then increases to a constant level on a 11 ps timescale. In addition to the ν = 0 → 1 transition, a weak ν = 1 → 2 hot band of CO_2 at ν = 2315 cm^{-1} is visible at short delays. The vibrationally excited CO_2 molecules relax to the vibrational ground state on a ~10 ps time scale. The modest population of the hot bands indicate that the majority of CO_2 molecules populate the vibrational ground state after 1 ps. The absorption dynamics after 1 ps therefore essentially reflects the CO_2 formation kinetics. The delayed appearance of CO_2 suggests that it is formed through a short-lived precursor, and the hot band indicate that the CO_2 molecules are formed in the hot environment surrounding the excitation site.

The appearance of CO_2 implies the formation of the alkaline CH_3CHOH^- counter fragment. The absorption associated with CH_3CHOH^- is expected to increase with time like the CO_2 counter product. The calculated intensities of CH_3CHOH^- listed in Table 2 are rather weak and with the possible exception of the transitions at ν = 1147 cm^{-1}, 1317 cm^{-1} and 1417 cm^{-1}, the predicted transitions of CH_3CHOH^- are hardly detectable by our transient absorption spectrometer. Nevertheless, accepting a Δν = 33 cm^{-1} (3 %) discrepancy between calculated and measured transition frequencies, the transient absorption observed in Fig. 5a, Fig. 5b and Fig. 6c at ν = 1180 cm^{-1} fit the predicted δOH transition frequency of CH_3CHOH^- and is as weak as expected from the calculated intensity. As expected, the δOH absorption increases with time, but the signal is too weak for a detailed comparison with the CO_2 dynamics. The calculations predict the transition frequency associated with the CH bending vibration of CH_3CHOH^- to ν = 1317 cm^{-1}, and this is in good agreement with the observed transient at ν = 1333 cm^{-1} displayed in in Fig 5c and Fig. 6d. The absorption dynamics of the ν = 1180 cm^{-1} and 1333 cm^{-1} transitions resemble that of CO_2 thus supporting the assignment to CH_3CHOH^-. The final CH_3CHOH^- transition, we may hope to see, is predicted at ν = 1417 cm^{-1}. The measured absorption at this frequency is dominated by the short-lived precursor. However, we note that a finite induced absorption at this frequency is present after the decay of the precursor. The agreement between measured and predicted absorption dynamics and frequencies of CH_3CHOH^- suggests that a substantial fraction of the lactate anions photo-dissociate to CH_3CHOH^- and CO_2, and that these species are present for more than t = 500 ps.

The CH_3CHOH^- moiety can disappear by one of two reactions. An intramolecular 1,2-hydrogen shift from the hydroxyl group to the carbon results in the formation of ethoxide:

$$h\nu + CH_3CHOHCO_2^- \rightarrow CH_3CHOH^- + CO_2 \rightarrow CH_3CH_2O^- + CO_2 \quad (1)$$

The hydrogen shift has a calculated barrier of 99 kJ/mol and a reaction energy of 177 kJ/mol. The ethoxide anion is weakly alkaline with pK_b=3.2 and is expected to be protonated to ethanol on time scales much longer than the 500 ps time span of the present measurements. Alternatively, CH_3CHOH^- can be protonated to give ethanol by a neighbouring water molecule:

$$h\nu + CH_3CHOHCO_2^- \rightarrow CH_3CHOH^- + CO_2 \xrightarrow{H_2O} CH_3CH_2OH + CO_2 + OH^- \quad (2)$$

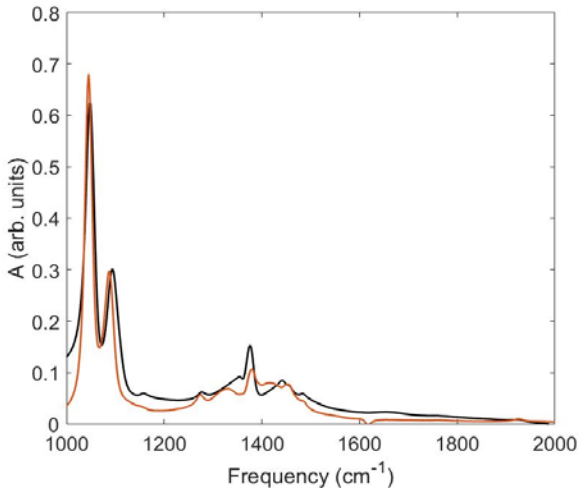

Fig. 7. ATR-FTIR spectrum of ethanol (red) and ethoxide (black).

Both of these reactions eventually lead to the formation of carbon dioxide and ethanol as indeed observed nearly a century ago.[13] The presence of a substantial energy barrier for reaction (1), compared to the essentially barrierless reaction (2), suggests that protonation of the strongly alkaline CH_3CHOH^- by water is the more likely reaction.

Reactions (1) and (2) could potentially be identified by the observation of ethoxide and ethanol, respectively. Fig. 7 shows the ATR-FTIR spectrum of ethoxide and ethanol in the region ν = 1000 – 2000 cm^{-1}. Ethoxide has three detectable transitions at ν = 1049 cm^{-1}, 1093 cm^{-1} and 1375 cm^{-1}. In ethanol, the same three transitions are found at ν = 1045 cm^{-1}, 1090 cm^{-1} and 1378 cm^{-1}. Ethoxide and ethanol are thus indistinguishable within the experimental uncertainty of the transient absorption spectrometer.

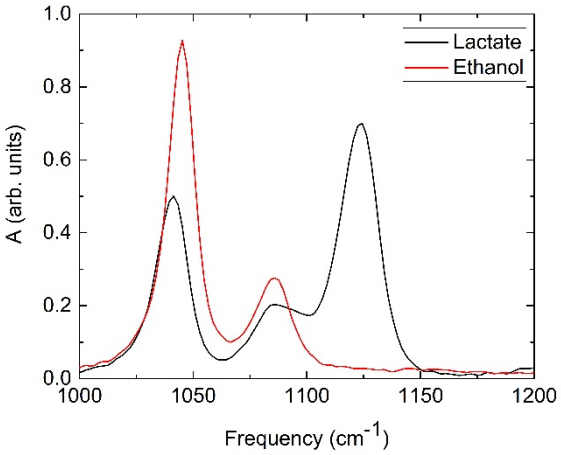

Fig. 8. ATR-FTIR spectra of 1.0 M lactate and 1.0 M ethanol in H2O.

Fig. 8 shows the ATR-FTIR spectra of aqueous ethanol and lactate. The ν = 1045 cm^{-1} and 1090 cm^{-1} transitions of ethanol coincide with the transitions associated with the νCC vibration of lactate, whereas the lactate transition at ν = 1125 cm^{-1} has no counterpart in ethanol. We utilize the spectra in Fig. 8 to assess the presence of ethanol among the photolysis products.

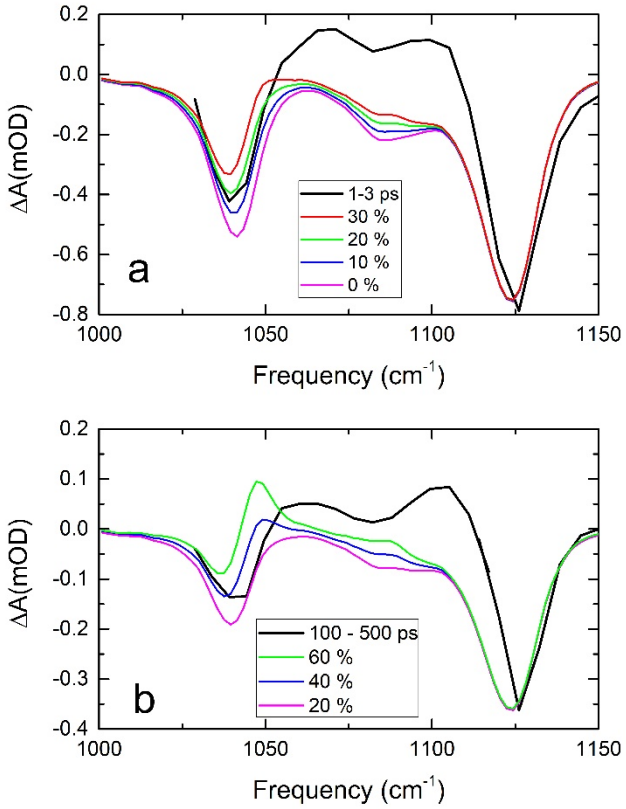

Fig. 9. a: Comparison of the transient absorption t = 1-3 ps after the excitation to calculated spectra for different ethanol yields. b: Comparison of the transient absorption data from t = 100-500 ps after the excitation to calculated spectra for different yields of ethanol.

Fig. 9a compares the transient absorption data shortly after the excitation to calculated spectra for different ethanol yields. To improve the statistics, we have averaged the transient data from t = 1-3 ps. The best agreement with the transient data is reached if 10-20 % of the excited lactate is converted to ethanol. However, this is likely an overestimate as the spectra of the transitions associated with the short-lived precursor at ν = 1060 cm^{-1} and 1094 cm^{-1} contribute to the transient absorption at ν = 1043 cm^{-1} and 1090 cm^{-1}. Likewise, Fig. 9b compares the transient absorption data from t = 100-500 ps after the excitation to calculated spectra for different yields of ethanol. The best agreement is obtained assuming 40 % of the lactate anions that have not returned to the ground state at this time have instead formed ethanol. Analysis of the transient data from t = 50-100 ps gives the same yield. The comparison between the transient absorption data and the FTIR data of ethanol thus shows that the transient data can accommodate contributions from ethanol, but ethanol accounts for less than half the excited lactate anions. As the spectra of ethanol and ethoxide are very similar, the same conclusions hold for ethoxide. The analysis thus suggests that CH_3CHOH^- is present throughout the t = 500 ps time span of our measurements, as indeed observed by the CH_3CHOH^- transitions at ν = 1180 cm^{-1}, 1333 cm^{-1} and 1435 cm^{-1} (the ESI contains more details regarding this analysis). As mentioned above, the CH_3CHOH^- is likely to be converted to ethanol by abstracting a proton from water, and there are evidences in the literature that this may occur on a time scale of hundreds of picoseconds.[38,39] We note that CH_3CHOH^- is formed in a dynamical process where the dissociating CO_2 likely perturbs the solvent cage, and this may influence the rate of proton abstraction.

In addition to CO_2, the experimental data in Fig. 5d reveal a weak induced absorption pertaining to the asymmetric stretch of $CO_2^{\bullet-}$ at ν = 1650 cm^{-1}. The absorption is present at all times, but its exact development is masked by the nearby negative absorption associated with ground state lactate. The formation of $CO_2^{\bullet-}$ implies the formation of the $CH_3CHOH^\bullet$ counter radical:

$$h\nu + CH_3CHOHCO_2^- \rightarrow CO_2^{\bullet-} + CH_3CHOH^\bullet \quad (3)$$

According to our calculations, the three strongest transitions of $CH_3CHOH^\bullet$ pertains to the mixed vibration at ν = 1031 cm^{-1}, the νC-O stretch at 1233 cm^{-1} and another mixed vibration at 1464 cm^{-1}. The strongest transition at ν = 1233 cm^{-1} is in full agreement with the 1230 cm^{-1} transition observed experimentally, while the predicted transitions at ν = 1031 cm^{-1} and 1464 cm^{-1} are obscured by the negative absorption associated with ground state lactate at ν = 1034 cm^{-1} and 1455 cm^{-1}, respectively. The remaining $CH_3CHOH^\bullet$ transitions are too weak to be detected. The absorption dynamics associated with ν = 1230 cm^{-1} transition of $CH_3CHOH^\bullet$ is shown in Fig. 6e. The absorption reaches 2/3 of its maximum value within 1 ps after the excitation pulse and continues to increase for another 10 ps before it drops to about half its maximum value after 100 ps. We will return to the $CH_3CHOH^\bullet$ absorption dynamics in the *Electron detachment* section. Considering the large calculated transition intensity of the $CO_2^{\bullet-}$ asymmetric stretch, the weak induced absorption indicate that dissociation into $CO_2^{\bullet-}$ and $CH_3CHOH^\bullet$ is only a minor channel.

Dehydroxylation

Our calculations (Fig. 2) suggest that in addition to decarboxylation, excitation of lactate at λ = 200 nm could also lead to dehydroxylation. The dissociation of the OH group can occur from the lowest excited state of lactate with a dissociation energy of 5.7 eV and with a barrier of ~0.3 eV. Considering that the excitation energy is 6.2 eV, dehydroxylation is energetically possible, and this would leave $CH_3CHCO_2^{\bullet-}$ as the counter anion.

$$h\nu + CH_3CHOHCO_2^- \rightarrow CH_3CHCO_2^{\bullet-} + OH^\bullet \quad (4)$$

Alternatively, the dissociation could lead to OH^- and the CH_3CHCO_2 molecule as the products, and calculations show that the latter closes to a lactone structure.

$$h\nu + CH_3CHOHCO_2^- \rightarrow CH_3CHCO_2 + OH^- \quad (5)$$

The IR spectral signatures of the hydroxide radical and anion are masked by the solvent, and identification of the dehydroxylation therefore depends on the detection of their counter products. The identification of the two dissociation channels is hampered by overlapping transitions of ground state lactate and potential photoproducts. However, the calculated spectrum of the CH_3CHCO_2 lactone has a strong carbonyl transition at ν = 1927 cm^{-1}, which stands out as a unique marker for the lactone and thereby for the dissociation of OH^- in reaction (5). As an experimental reference, we note that the measured spectrum of β-propiolactone vapor and liquid have very strong carbonyl stretching transitions at ν = 1882 cm^{-1} and 1832 cm^{-1}, respectively.[40] The transient absorption depicted in Fig. 5e show no absorption features in the spectral range ν = 1750 cm^{-1} - 2100 cm^{-1} and lactate is thus unlikely to dissociate into CH_3CHCO_2 and OH^-.

Within the calculation uncertainty, the spectrum of the $CH_3CHCO_2^{\bullet -}$ anion in reaction (4) share many of the transition frequencies with ground state lactate and some of the product species. Nevertheless, the strong asymmetric CO_2^- stretch of the $CH_3CHCO_2^{\bullet -}$ anion calculated at ν = 1550 cm^{-1} is shifted by $\Delta\nu$ = 63 cm^{-1} relative to that of ground state lactate and seems a good marker for reaction (4). We have already accounted for all absorption features within $\Delta\nu$ = 100 cm^{-1} of ν = 1550 cm^{-1} and the $CH_3CHCO_2^{\bullet -}$ radical anion is therefore not observed. This suggests that dehydroxylation of lactate is only a very minor reaction channel, if the reaction occurs at all. Fig. 2a, b, c can rationalize this observation by assuming that decarboxylation is faster than dehydroxylation for dynamical reasons, despite the fact that both reactions have similar energetic barriers.

Short-lived precursor

The recorded data of lactate show six positive short-lived absorption transients at ν = 1060 cm^{-1}, 1094 cm^{-1}, 1270 cm^{-1}, 1301 cm^{-1}, 1387 cm^{-1} and 1435 cm^{-1} assigned to the species we coined precursor. We have calculated the IR spectra for a range of conceivable molecular species related to lactate, but only the lowest excited singlet state of the lactate anions was found to provide a satisfactory match. We will thus argue that the short-lived precursor most likely is the lowest excited singlet state.

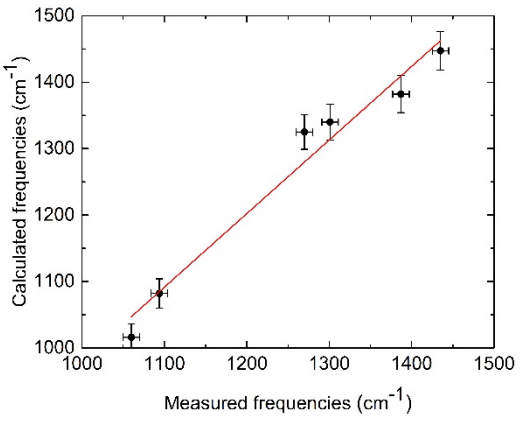

Fig. 10. Comparison between the measured transition frequencies of the short-lived precursor and the calculated transition frequencies of the lowest excited singlet state of lactate.

Fig. 10 compares the measured transition frequencies of the short-lived precursor to calculated transition frequencies of the lowest excited singlet state of lactate. The red line is the best linear fit to the data with a slope of α = 1.1 and R^2 = 0.97. The good correlation between measured and calculated values indicate that the short-lived precursor is the lowest excited singlet state. The calculated transitions of the lowest excited singlet state at ν = 1114 cm^{-1}, 1135 cm^{-1} and 1409 cm^{-1} are not discernable from other absorption transients in the experimental data. Fig. 6b shows the time dependence of the absorption associated with the lowest excited singlet state exemplified by the transient at ν = 1435 cm^{-1}. The absorption is present after t = 1 ps and increases for another 1.4 ps to peak at 2.4 ps. The 6.2 eV photon energy populates a number of excited states (Fig. 2) and the initial absorption increase likely reflects the relaxation to the lowest excited state. Subsequently, the transient absorption drops to a constant level on a 11 ps time scale. The first 100 ps of the transient absorption pertaining to CO_2 is depicted in Fig. 6f. The τ = 11 ps time constant for the CO_2 increase is identical to the 11 ps decay of the lowest excited state suggesting that CO_2 is formed by dissociation from this state.

Electron detachment

Considering that the anionic electron is located on the carboxylate group it is counter intuitive that decarboxylation predominantly leads to the formation of CO_2 whereas the intuitively more likely dissociation product of $CO_2^{\bullet -}$ only constitute a minor channel. Although being a stable molecule, aqueous $CO_2^{\bullet -}$ has a detachment energy of only ~ 0.28 eV in bulk water and studies of $CO_2^{\bullet -}$ in water clusters find a vertical detachment energy of 0.48 eV and an adiabatic electron affinity of 0.12 eV.[41-43] We therefore speculate that, the dissociating $CO_2^{\bullet -}$ fragment detaches the electron concurrently with the dissociation as it interacts with the hot environment surrounding the excitation site.

$$h\nu + CH_3CHOHCO_2^- \rightarrow CH_3CHOH^{\bullet} + CO_2 + e^- \quad (6)$$

If the ejected electron becomes hydrated in the surrounding water it develops a wide absorption spectrum ranging from UV to near IR with a temperature dependent maximum around λ = 720 nm.[44,45] In order to investigate the potential electron detachment from $CO_2^{\bullet -}$ during the dissociation of lactate, we have recorded the formation of hydrated electrons with UV-Vis transient absorption spectroscopy by probing the hydrated electrons at 650 nm. It is in general challenging to identify hydrated electrons from aqueous solutes excited by intense ultraviolet light pulses because, as already discussed in the *Protonation by secondary reactions* section, hydrated electrons produced by non-linear ionization of the water molecules often mask the electrons from the solute.[37,46] Nevertheless, in the case of aqueous lactate, the analysis in the ESI shows that it is possible.

The linear contribution of electrons from lactate to the absorption at λ = 650 nm stands out when the pump pulse energy is reduced by an order of magnitude to 0.23 μJ as shown in Fig. 11. Here it is clear that the initial sub-picosecond rise in the absorption associated with the electron concentration is followed by a double exponential decay with two time constants τ_1 = 1.2 ps and τ_2 = 20 ps. Fitting a single exponential function to the electron concentration results in a time

constant of τ = 14 ps comparable to the 11 ps time constant of the increase in the CO_2 concentration.

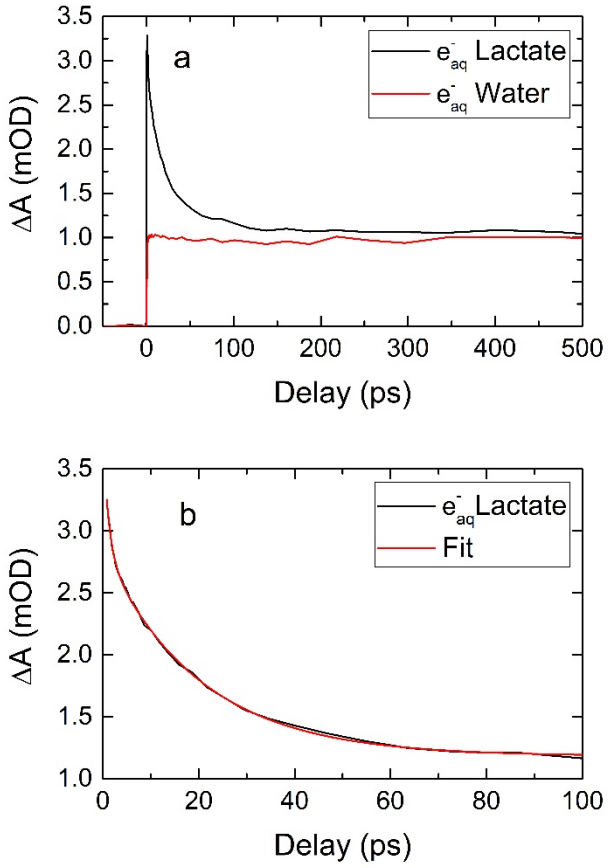

Fig. 11. a: The transient absorption associated with hydrated electrons measured at λ = 650 nm. The hydrated electrons results from photo-excitation of water and aqueous lactate with λ = 200 nm pulses with a pulse energy of 0.23 μJ. b: The decay of the electron concentration is well-described by a double exponential function ΔA = 1.2 mOD + 0.92 mOD ×exp(-t/1.2 ps) + 1.68 mOD × exp(-t/20 ps).

The drop in the electron concentration indicates that the detached electron reacts with one of the two dissociating products. The carbon dioxide fragment is a stable molecule unlikely to recombine with the electron. This is consistent with the monotonic increase of the infrared absorption associated with CO_2 shown in Fig. 5f and Fig. 6f. The $CH_3CHOH^\bullet$ counter product, on the other hand, is an unstable radical prone to react with the nearby hydrated electron thereby forming CH_3CHOH^-:

$$CH_3CHOH^\bullet + e_{aq}^- \rightarrow CH_3CHOH^- \quad (7)$$

The CCSD(T)/aug-cc-pV(T,Q)Z extrapolated attachment energy for the vertical reaction (7) with one explicit water molecule is 1.5 ± 0.1 eV, which is comparable to the $\Delta G_{hyd}^{298}(e^-)$ = 1.48 eV of the hydrated electron.[47] Geometry relaxation of the formed anion further increases the electron attachment energy by 0.8 eV, and this makes electron attachement to the $CH_3CHOH^\bullet$ radical energetically viable. The $CH_3CHOH^\bullet$ concentration is thus expected to drop on a τ_2 = 24 ps timescale, while the CH_3CHOH^- concentration is expected to increase, and this is confirmed by the transient absorption data in Fig. 6c-e. The absorption associated with the ν = 1230 cm^{-1} transition of $CH_3CHOH^\bullet$ shown in Fig. 6e reaches its maximum value in 10 ps before it drops to about half its maximum value after 100 ps. The absorption associated with the ν = 1180 cm^{-1} and 1333 cm^{-1} transitions of CH_3CHOH^- depicted in Fig. 6c and Fig. 6d increase on the same time scale, and this substantiates reaction (7). The inferred mechanism is that CO_2 is formed during decarboxylation of lactate with simultaneous ejection of an electron and it is subsequently transferred to the $CH_3CHOH^\bullet$ counter product.

In addition to dissociation, the *Introduction* mentions electron detachment as a potential outcome of the photo-excitation of lactate anions at λ = 200 nm.

$$hv + CH_3CHOHCO_2^- \rightarrow CH_3CHOHCO_2^\bullet + e^- \quad (8)$$

The calculated vertical electron detachment energy is 6.6 ± 0.1 eV or 7.2 eV if three explicit water molecules are included. These values exceed the excitation energy of 6.2 eV and direct electron detachment is therefore unlikely. This is consistent with the UV-IR transient absorption data: Electron detachment of lactate anions potentially leads to the formation of lactate radicals (8), and our calculations indicate that this in a barrier-less reaction dissociates into CO_2 and $CH_3CHOH^\bullet$.

$$CH_3CHOHCO_2^\bullet \rightarrow CH_3CHOH^\bullet + CO_2 \quad (9)$$

The products after direct electron detachment of lactate are thus the same as for decarboxylation with simultaneous ejection of an electron. If reaction (9) occurs in less than 1 ps as expected, the absorption dynamics of the products from reaction (8) and reaction (9) is indistinguishable from that of reaction (6). However, as argued in the *short-lived precursor* section, the observed decarboxylation process occurs via the lowest singlet excited state of lactate and this state does not correlate with direct electron detachment. Consequently, the observed decarboxylation is not resulting from direct electron detachment.

Quantum Yields for photo-dissociation

Fig. 6a shows that the absorption associated with ground state lactate recovers to a constant level within 100 ps. Fig. 6b furthermore shows that the short-lived transients disappear within 100 ps and Fig. 6c shows that the absorption associated with the formation of CO_2 is constant after 100 ps. The primary photochemistry of lactate has thus ended 100 ps after the excitation pulse. We can therefore derive the quantum yields for the photo-dissociation of aqueous lactate from the transient absorption data. Since the absorption of one 200 nm photon results in the excitation of one lactate molecule, we define the primary photo-dissociation quantum yield, Φ(t), as the fraction of molecules excited at *t*=0 that has not returned to the electronic ground state at a later time *t*. If the lactate ground state is the only absorber at a particular frequency, the quantum yield can be derived from the transient data as $\Phi(t) = \Delta A(t)/\Delta A(t=0)$. To a good approximation this is fulfilled by the transitions at ν = 1117 cm^{-1} and 1570 cm^{-1} during the first 100 ps. From the transition at ν = 1117 cm^{-1} we find that Φ(100 ps) = ΔA(100 ps)/ ΔA(1ps) = 38±5 % of the

excited lactate remain dissociated after 100 ps. The primary photo-dissociation quantum yield derived from the absorption recovery of the transition at 1570 cm^{-1} is $\Phi(100\ ps) = \Delta A(100\ ps)/\ \Delta A(1ps) = 41\pm5$ % in good agreement with the value derived from the transition at ν = 1117 cm^{-1}. The dissociation quantum yield of lactate is close to that of the six carboxylates mentioned in the *Introduction* and likely carries over to other carboxylates as well.

Conclusion

Our combined experimental and theoretical results suggest that irradiation at 200 nm of aqueous lactate populates one or more excited states, which decay to the lowest excited singlet state within 2.4 ps. The lowest excited state remains populated for about 11 ps before it either dissociates to carbon dioxide or return to the electronic ground state. The experimental results show that about 40% of the excited molecules dissociate, while the remaining molecules return to the electronic ground state and vibrationally equilibrate on a ~10 ps timescale. During the dissociation process the electron is transferred from the carboxylate site to the counter radical $CH_3CHOH^{\bullet}$ to yield CH_3CHOH^{-}. CH_3CHOH^{-} is likely to be converted to ethanol by abstracting a proton from water but our transient absorption data cannot quantify the amount due to spectral overlap. The experimental and computational results show no indication of lactate losing an electron by direct photo-detachment upon irradiation at 200 nm.

We recently reported the photolysis of aqueous formate, acetate propionate, alanine, isoleucine and proline at 200 nm. The data showed dissociation dynamics very similar to those of lactate in the present work, with decarboxylation via a short-lived lowest excited state as the primary reaction channel. Both time scales and dissociation yields of around the 40 %, as well as the calculated excited state surfaces, are very similar. Even the absorption dynamics of CO_2 following the dissociation is nearly identical in all the species. This suggests that $n_O \rightarrow \pi_{CO}^*$ excitation at 200 nm of the carboxylate group leading to decarboxylation is a general reaction channel. Since decarboxylation of the isolated species is virtually barrier-less and thus suggests 100 % dissociation yield, the 40 % yield likely reflects the surrounding water solvent's ability to induce the internal conversion from the lowest excited state to the ground state during the ~11 ps lifetime of the excited state. In the amino acids and lactate, calculations indicate that decarboxylation is only one of two possible dissociation channels. In the amino acids, the calculations predict nearly barrier-free deamination and in lactate they suggest also a similar low barrier for dehydroxylation. However, despite careful investigations these dissociation channels have not been identified experimentally. This may indicate that decarboxylation is the fastest of the three dissociation channels and therefore closes the window of opportunity before deamination of amino acids and dehydroxylation of lactate have time to occur, and this can be rationalized from the computational results. In this scenario, the photolysis is entirely determined in the carboxylate chromophore end of the molecules, while the other parts of the molecule remain passive.

The photo-induced decarboxylation of lactate is thus in line with the observed photo-decarboxylation of amino acids and simple carboxylates. It implies that fully exposed to the ultraviolet light from the young sun,[48,49] these prebiotic species were constantly dissociated with yields approaching 40 % generating organic radical species and carbon dioxide as the dominating product. On ancient Earth, production of $OH^{\bullet}$ radicals would have been limited to water dissociation and therefore it is likely that organic radicals generated photochemically from prebiotically available targets were important in the formation of complex molecules.[6,50] Our studies of the primary ultraviolet photolysis of carboxylates and amino acids show that the same ultraviolet irradiation that causes decarboxylation of these species also generate a host of reactive organic radicals that in turn can initiate the more complex organic chemistry necessary for life.

Conflicts of interest

There are no conflicts to declare.

Acknowledgements

We thank Brianna Hopper and Alexandra Deal for discussions concerning the ultraviolet absorption spectrum of aqueous lactate. We also would like to acknowledge insightful discussions about reaction mechanisms with Barry Carpenter.

VV acknowledges partial support by the U. S. Army Research Office under the grant no. ARO W911NF1710115 and the National Science Foundation grant no. CHE 1611107

References

1 C. Chyba and C. Sagan, *Nature*, 1992, **355**, 125.
2 A. Knoll, *Life on a Young Planet: The First Three Billion Years of Evolution on Earth.* Princeton University Press, Princeton, 2003, pp. 1–277.
3 F. Westall and A. Brack, *Space Science Reviews*, 2018, **214**, 1.
4 S. L. Miller, *Science*, 1953. **117**, 528.
5 S. L. Miller and H. C. Urey, *Science*, 1959, **130**, 245.
6 R. J.Rapf and V. Vaida, *Phys. Chem. Chem. Phys*. 2016, **18**, 20067.
7 C. M. Dobson, G. B. Ellison, A. F. Tuck and V. Vaida, *PNAS*, 2000, **97**, 11864.
8 Griffith, E. C., Tuck, A. F., Vaida, V. *Acc. Chem. Res*. 2012, **45** 2106.
9 F. I. Kasting, *Science.* 1993, **259**, 5097.
10 S. Ranjan and. D. D. Sasselov, *Astrobiology* 2016, **16**, 68.
11 M. M. Madsen, F. Jensen, S. J. Knak Jensen and J. Thøgersen *Phys. Chem. Chem. Phys.*,2019, **21**, 7358.
12 M. M. Madsen, F. Jensen, S. J. Knak Jensen and J. Thøgersen *Phys. Chem. Chem. Phys.*2020, **22**, 2307.
13 G. R. Burns, *Journ. Am. Chem. Soc.* 1929, **52**, 5272.
14 H. Harada, T. Sakata and T. Ueda. J. Am. Chem. Soc. 1985, **107**, 1773.

15 H. Harada, T. Sakata and T. Ueda, *J. Phys. Chem.* 1989, **93**, 1542.
16 T. Sakata. *J. Photochem.*, 1985, **29**, 205.
17 A. V. Puga, *Coord. Chem. Rev.* 2016, **315**, 1.
18 K. Liu, A. Litke, Y Su, B. v. Campenhout, E. A, Pidko, E. J. M. Hensen. *Chem. Commun*. 2016, **52**, 11635.
19 J. Thøgersen, J. Rehault, M. Odelius, T. Ogden, N. K. Jena, S. J. Knak Jensen, S. R. Keiding and J. Helbing. *J. Phys. Chem. B*. 2013, **117**, 3376.
20 B. Frandsen, N. Benjamin, A. M. Deal, J. R. Lane and V. Vaida. *J. Phys. Chem. A* 2021 **125**(1), 281.
21 J. –D. Chai, M. Head-Gordon, *Phys. Chem. Chem. Phys.* 2008, **10**, 6615.
22 F. Jensen, *J. Chem.Theory Comp*., 2014, **10**, 1074.
23 M. J. Frisch, G. W. Trucks, H. B. Schlegel, G. E. Scuseria, M. A. Robb, J. R. Cheeseman, G. Scalmani, V. Barone, G. A. Petersson, H. Nakatsuji, X. Li, M. Caricato, A. V. Marenich, J. Bloino, B. G. Janesko, R. Gomperts, B. Mennucci, H. P. Hratchian, J. V. Ortiz, A. F. Izmaylov, J. L. Sonnenberg, D. Williams-Young, F. Ding, F. Lipparini, F. Egidi, J. Goings, B. Peng, A. Petrone, T. Henderson, D. Ranasinghe, V. G. Zakrzewski, J. Gao, N. Rega, G. Zheng, W. Liang, M. Hada, M. Ehara, K. Toyota, R. Fukuda, J. Hasegawa, M. Ishida, T. Nakajima, Y. Honda, O. Kitao, H. Nakai, T. Vreven, K. Throssell, J. A. Montgomery, Jr., J. E. Peralta, F. Ogliaro, M. J. Bearpark, J. J. Heyd, E. N. Brothers, K. N. Kudin, V. N. Staroverov, T. A. Keith, R. Kobayashi, J. Normand, K. Raghavachari, A. P. Rendell, J. C. Burant, S. S. Iyengar, J. Tomasi, M. Cossi, J. M. Millam, M. Klene, C. Adamo, R. Cammi, J. W. Ochterski, R. L. Martin, K. Morokuma, O. Farkas, J. B. Foresman, and D. J. Fox, Gaussian, Inc., Wallingford CT, 2016.
24 D. Jacquemin, V. Wathelet, E. A. C. Adamo. *J. Chem. Theory Comput.* 2009, **5**, 2420.
25 A. D. Laurent and D. Jacquemin, *Int. J. Quant. Chem*., 2013, **113**, 2013.
26 M. Isegawa, R. Peverati. D. Truhlar. *J. Chem. Phys.* 2012, **137**, 244104.
27 D. Jacquemin, E. A. Perpète, I. Ciofini, C. Adamo. *Theor. Chem. Acc.*, 2011, **128**, 127.
28 M. Falk and A. G. Miller, *Vibrational Spectroscopy.* 1992, **4**, 105.
29 M. Zhou and L Andrews. *J. Chem. Phys.* 1999, **110**, 2414.
30 M. E. Jacox and W. E. Thompson, *J. Chem. Phys.*, 1989, **91**, 1410.
31 J. T. Godbout, T. M. Halasinski, G. E. Leroi, and J. Allison, *J. Phys. Chem.*, 1996, **100**, 2892.
32 A. Herburger, M. Oncák, C. Siu, E. Demissie, J. Heller, W. Tang, M. Beyer. *Chem. Eur J .* 2019, **25**, 10165.
33 M. Møller Madsen, F. Jensen, S. J. Knak Jensen and J. Thøgersen, Phys*. Chem. Chem. Phys.*, 2019, **21**, 7358.
34 M. Pecul. A. R. J. Leszczynski *J. Phys. Chem. A.,* 2002, **106***,* 11008-11016.
35 S. Burikov, T. Dolenko, S. Patsaeva, Y. Starokurov, V. Yuzhakov, *Mol. Phys.*, 2010, **108**, 2427.
36 J. Thøgersen, A. Colette, S. R. Keiding, F. Jensen, S. V. Hoffmann, N. Jones and S. J. Knak Jensen. *Phys. Chem. Chem. Phys.*, 2017, **19**, 1560.
37 C. G. Elles, A. E. Jailaubekov, R. A. Crowell, S. E. Bradforth. *J. Chem. Phys.* 2016, **125**, 44515.
38 M. J. Cox and H. J. Bakker. *J. Chem. Phys.* 2008, **128**, 174501.
39 S. R. Keiding, D. Madsen, J. Thøgersen. *Chem. Phys. Lett.*, 2004, **390**, 94.
40 J. R. Durig. *Spectrochim. Acta.* 1963, **19**, 1223.
41 I. Jannik and G. N. R. Tripathy, *J. Chem. Phys.* 2016, 144, 154307.
42 J. Kim, I. Becker, O. Cheshnovsky and M. A. Johnson*. Chem. Phys. Lett.* 1998, **297**, 90.
43 B. M. Elliiot, L. R. McCunn and M. A. Johnson. *Chem. Phys. Lett.* 2008, **467**, 32.
44 J. W. Boag and E. J. Hart. *Nature*, 1963, 197, 45.
45 F.-Y. Jou and G. R. Freeman, *J. Phys. Chem.* 1977, **81**, 909.
46 C. L. Thomsen, D. Madsen, S. R. Keiding and J. Thøgersen. *J. Chem. Phys.* 1999, **110**, 3453.
47 C-G. Zhan and D. A. Dixon. *J. Chem. Phys. B*. 2003, **107**, 4403.
48 M. W. Claire, J. Sheets, M. Cohen, I. Ribas, V. S. Meadows and D. C. Catling. *Astrophys. Journ*. 2012,**757**, 1.
49 M. Canuto, J. S. Levine, T. R. Augustsson and C. L. Imhoff, *Nature*, 1982, **296**, 816.
50 R. J. Rapf, R. J. Perkins, M. R. Dooley, J. A. Kroll, B. K. Carpenter and V. Vaida. *ACS central Science*, 2018, **4**, 624.